Electrochimica Acta 540 (2025) 146907

Contents lists available at ScienceDirect

Electrochimica Acta

journal homepage: www.journals.elsevier.com/electrochimica-acta

Electrochemical picobalance: Proof-of-principle for an electrochemical cantilever-based mass balance

Nadine Raßmann [a], Roman E. J. Glaß [a], Nicolas Helfricht [a,b], Georg Papastavrou [a,b,c,*]

[a] Physical Chemistry II: Interfaces and Nanoanalytics, University of Bayreuth, Universitätsstraße 30, 95447 Bayreuth, Germany
[b] Bavarian Polymer Institute, University of Bayreuth, Universitätsstraße 30, 95447 Bayreuth, Germany
[c] Bayreuth Center of Colloids and Interfaces, Universitätsstraße 30, 95447 Bayreuth, Germany

ARTICLE INFO

Keywords:
Atomic force microscopy
Scanning electrochemical force microscopy
Cantilever
Electrochemical deposition
Chronoamperometry
Electrochemical quartz crystal microbalance

ABSTRACT

Since the introduction of Faraday's law, the combination of electrochemical methods with gravimetric techniques has been pursued very actively in the field of electrochemistry. Here, we present a proof-of-concept to combine electrochemical methods with the recently introduced picobalance, which originates from atomic force microscopy (AFM). The picobalance is a cantilever-based technique that can measure mass changes in the order of a few picograms. The development of fully insulated cantilevers with an integrated microelectrode (electrochemical balance probes, EBPs) was an essential prerequisite for the electrochemical picobalance. The electrochemical deposition of copper allowed for a highly defined and continuous deposition of mass on the EBP. By comparing the faradaic current and the mass signal of the picobalance, the mass sensitivity of the latter has been determined as 4.6 fg·μm^{-2}·Hz^{-1} (or ~ 460 ng·cm^{-2}·Hz^{-1}). This value can be readily compared to the one for the electrochemical quartz microbalance (EQCM), which has been used here as a benchmark under the same conditions (17.5 ng·cm^{-2}·Hz^{-1}). However, in contrast to the EQCM, the picobalance is capable of measuring absolute masses as low as one picogram. The here-presented electrochemical picobalance allows for applications in electropolymerization, organic electronics, and bioelectrochemistry.

1. Introduction

Material deposition on electrodes is a universal process in electrochemistry, which is often referred to as electrodeposition [1,2]. Starting with Faraday, mass deposition was essential for developing electrochemical concepts [3]. Faraday's law of electrolysis states a direct relation between the transferred charge at the interface of an electrode and the deposited mass of a metal [1,3]. Historically, Faraday established it based on experimental data for the deposition of copper onto macroscopic electrodes. The mass change was determined gravimetrically [1,3]. Following this landmark experiment, gravimetric detection by the associated faradaic current became a standard technique in electrochemistry [4–7], biomedical sensing [8], and energy storage applications [9–11].

Electrochemistry has a long history of being integrated with various surface analytical techniques to further characterize the solid/liquid interface of an electrode under potentiostatic control. Examples include IR-spectroscopy, optical microscopy, ellipsometry, X-ray, reflectometry, and atomic force microscopy (AFM) [5,12–17]. One technique that allows for directly determining the mass deposited on an electrode is the quartz crystal microbalance (QCM), which is among the most utilized surface analytical techniques in combination with electrochemistry [4,9,18]. The QCM dates back to the early experiments of Sauerbrey in the 1950s, who employed the inverse piezoelectric effect for microgravimetric studies [19]. The QCM detects a piezoelectric resonator's frequency or amplitude shift due to the deposited mass [20]. Originally, QCMs have been primarily used in the gas phase and are still employed as a monitoring device to determine the mass deposited by physical vapor deposition, such as thermal evaporation or sputter coating [21,22]. According to the Sauerbrey equation, the deposited mass and the resulting frequency shift are directly proportional [19]. However, this equation is only valid for sufficiently thin and rigid layers.

The principle of QCM also allows for the operation in liquid environment [20,23,24]. QCM in liquid enables not only for applications such as biosensing [25] but also to follow interfacial electrode processes [4,9,18,26–29]. In this respect, electrochemical deposition with Faraday's law is often used to calibrate electrochemical QCM (EQCM) setups or new resonator designs [30–32]. It should be noted that for a QCM

* Corresponding author.
E-mail address: georg.papastavrou@uni-bayreuth.de (G. Papastavrou).

https://doi.org/10.1016/j.electacta.2025.146907
Received 20 March 2025; Received in revised form 7 July 2025; Accepted 11 July 2025
Available online 22 July 2025

operated in liquid, water will also be bound to the surface of the QCM sensor while it is oscillating. Tightly bound water can include much more than only ions of the double layer, especially when extended layers of organic material protrude into the solution [24]. Hence, QCM in liquid determines the so-called wet mass in contrast to other techniques such as optical reflectometry [24,33]. In the case of extended layers, hydrodynamic damping can be used to estimate properties, such as thickness and elastic behavior [20]. One technique used to address hydrodynamic damping is referred to as QCM with dissipation monitoring (QCM-D) and is based on short excitation sequences to the sensor, whose subsequent damping is followed [24,34]. QCM-D has also been used in combination with electrochemistry, for example, in the context of electropolymerization [35,36] and electrogelation [37,38].

Recently, a new technique to determine masses and mass changes of isolated, micrometer-sized objects has been introduced. This technique is founded on AFM and is often referred to as picobalance [39]. The picobalance is also based on the resonance shift of a mechanical microresonator like the QCM. However, in contrast to the shear oscillations of a QCM crystal, the picobalance is based on the oscillations of a cantilever commonly used in atomic force microscopy (AFM) [39,40]. The cantilever oscillations are induced by photothermal excitation using a modulated IR laser focused near the clamped end of the cantilever beam [41,42]. The cantilever's deflection during oscillation is read out by an additional laser that is reflected on the free end of the cantilever (optical light lever technique) [43]. Any changes in the mass immobilized at the end of the cantilever result in a change of its resonance frequency. Recording frequency sweeps with and without an attached mass and fitting the respective phase and amplitude response with a driven and damped oscillator yields the resonance frequency. The mass can then be calculated from the difference in natural frequency. The corresponding frequency shift can also be detected continuously using a phase-locked loop (PLL). The PLL maintains a constant phase shift of 90° by adjusting the excitation frequency in accordance with the mass change at the cantilever.

Originally, the picobalance was developed with the aim to detect the mass fluctuation in single living cells with millisecond and piconewton resolution over time scales of days [39]. So far, the picobalance has mainly been employed in a biological context [40,44–46]. It should be noted that other microresonators are sometimes also referred to as 'picobalances'. However, these techniques are not AFM-based [47,48].

Electrochemistry has a long history of hyphenating with other techniques, such as ellipsometry, spectroscopy, and QCM. Here, we developed the electrochemical picobalance, which adds another gravimetric technique that is sensitive to the smallest mass changes on an absolute scale. Within this feasibility study, we demonstrated by electrochemical techniques that indeed the mass resolution of the AFM-based picobalance is on the order of 1 picogram. The preparation of special AFM cantilevers, which could also act as electrochemical sensors bearing integrated µm-sized electrodes [49,50], has been further developed and adapted to the requirements for the picobalance measurements. In our proof-of-feasibility of an electrochemical picobalance, we show that Faraday's law of electrolysis can also be used to correlate current and deposited mass. Thus, 'classical' electrochemical techniques, such as cyclic voltammetry and chronoamperometry, can be readily combined with the picobalance setup. With the advent of organic electronics and the strong current interest in electrically addressing cells, the combination of electrochemistry and picobalance will open new possibilities for single-cell electrochemistry [51,52]. Moreover, the picobalance technique will allow for overcoming hydrodynamic limits of EQCM for electropolymerization and electrogelation when thick polymer films are present on the sensor [24,53].

2. Experimental

2.1. Fabrication of electrochemical balance probes

The electrochemical balance probes for the picobalance were fabricated from commercial gold-coated tipless AFM cantilevers (HQ:NSC35-C/tipless/Cr-Au, MikroMasch, Sofia, Bulgaria). These cantilevers have a nominal spring constant of 5.4 Nm^{-1} and a nominal resonance frequency of 150 kHz. The two lever arms, which were not used, i.e., NSC35-A and B on the chip, were removed beforehand. We modified a previously published procedure for the preparation of electrochemical colloidal probes [49] to meet the requirements for our microelectrode mass sensors. The cantilevers were electrically contacted and, afterward, completely insulated, leaving an approximately circular gold electrode area uncoated.

Briefly, the cantilevers were cleaned by dipping them alternatingly in MilliQ water (resistivity >18 MΩcm, Merck Millipore, Darmstadt, Germany) and EtOH (p.A., VWR, Darmstadt, Germany). Subsequently, the cantilevers were exposed to air plasma (Zepto, Diener Electronics, Ebhausen, Germany) for 180 s, dipped into EtOH, and left to dry in air. The later electro-active area, i.e., the microelectrode, had been protected by spherical polystyrene particles (PS, with a nominal diameter of 30 µm, microparticles, Berlin, Germany). This sacrificial particle masked the future electrode area during the following insulating steps and was successively removed after finalizing the insulating process. For this purpose, a PS microsphere (nominal diameter 30 µm, PS-R-30.0, Microparticles, Berlin, Germany) was placed on the free end of the cantilever using a micromanipulator (DC-3 K, Märzhäuser, Ebhausen, Germany) equipped with etched tungsten wires under the control of an optical fixed-stage microscope (Axio Examiner D1, Zeiss, Oberkochen, Germany). The particle transfer and immobilization are enabled by capillary forces. A similar approach has been reported previously by us for the preparation of electrochemical colloidal probes [49]. Afterward, the cantilever was tempered at 200 °C in a reflux oven for 180 s (Protoflow S, LKPF Laser, and Electronics AG, Garbsen, Germany) to increase the contact area of the priorly placed PS particle. Furthermore, electrical contact was established by attaching a polyimide-insulated silver wire (0.125 mm, Advent Research Material, Oxford, United Kingdom, insulation partially removed) to the cantilever chip using conductive silver paint (Acheson silver DAG 1415, Plano, Marburg, Germany). A small droplet of UV curable glue (NOA 63, Norland Products, Cranbury, USA) was applied to the contact to seal it electrically and provide mechanical support. The cantilever chip was insulated by carefully dipping it into 1:1 (w:w) diluted red insulating varnish (4228, MG Chemicals., Burlington, Canada) with the dedicated thinner (4354, MG Chemicals, Burlington, Canada) using a micromanipulator under optical control with a digital microscope (Supereyes, Shenzhen Supereyes Co. Ltd., Shenzhen, China). After drying at room temperature for >12 h, the insulating coating was cured in a reflux oven at 80 °C for 1 h.

The cantilever was insulated using a cathodic paint (ClearClad HSR, LHV coatings, Birmingham, United Kingdom). For this purpose, the paint was diluted 1:5 in MilliQ water, stirred for >24 h, and filtered through a syringe filter (PES, hydrophilic, 0.22 µm, Carl Roth, Karlsruhe, Germany) immediately before use. The paint was deposited in a two-electrode configuration with a platinum sheet (15 mm^2, 99.95 %, Goodfellow, Hamburg, Germany) acting as the counter electrode. The deposition was conducted three times at −3.0 V for 120 s using a potentiostat (PGU BI-1000, Ingenieurbüro Peter Schrems, Münster, Germany). The cantilevers were gently dipped in MilliQ water before and after every deposition step. After the third step, the cantilever was removed from the suspension without being dipped into MilliQ water. It was left to dry at room temperature for 15 min before curing the coating at 160 °C for 20 min in a reflux oven. This deposition cycle was repeated three times. Finally, the sacrificial PS microsphere was removed from the cantilever using a micromanipulator equipped with an etched tungsten wire. Due to the masking effect of the PS particle during the

different insulating steps, an approximately circular non-insulated gold electrode at the free end of the cantilever was obtained (cf. Fig. 1C and Fig. S5). We refer to these cantilevers with integrated electrodes in the electrochemical picobalance experiments as 'electrochemical balance probes' (EBP).

The spring constants of the used EBPs were calibrated according to the procedure introduced by Cleveland et al. [54] after the electrodeposition or added mass experiments. Briefly, a minimum of 7 individual tungsten beads were picked up with each cantilever under ambient conditions. The micropheres adhered to the EBPs, primarily due to capillary forces. The spring constant was determined from the shift of the resonance frequency and the theoretical particle mass, calculated from the bead diameter and particle position on the cantilever, which was determined by optical microscopy for each attached particle.

2.2. Picobalance setup

The picobalance setup is based on a commercial AFM (DriveAFM, Nanosurf AG, Liestal, Switzerland) equipped with a CX controller (Nanosurf AG, Liestal, Switzerland). Two different lasers are available in the used AFM: 1) a photothermal excitation laser (CleanDrive, $\lambda = 785$ nm), which drives the cantilever's oscillation, and 2) a readout laser ($\lambda = 840$ nm) to detect the cantilever deflection. Optical control is realized by placing the AFM setup on top of an inverted optical microscope (Axiovert 200, Zeiss, Oberkochen, Germany). A commercial fluid cell (Asylum Research, Oxford Instruments, Santa Barbara, USA) with exchangeable glass bottom discs (diameter 35 mm, Irlbacher Blickpunkt Glas, Schönsee, Germany) was used for measurements in liquid.

2.3. Resonance shifts by added mass

The mass sensing by the electrochemical balance probes was verified by attaching tungsten microspheres ($\rho = 19.25$ g·cm^{-3} [55]) with variable sizes to the modified electrochemical cantilevers in 0.1 mM aqueous HCl pH 4 (Titrisol, Sigma-Aldrich, Merck, Darmstadt, Germany). The mass determined by the picobalance has been compared to the theoretical mass calculated based on the dimensions and density of the respective particles.

The electrochemical balance probes were exposed to UV/ozone treatment (UVO—Cleaner, Jelight Co. Inc., Irvine, USA) for 10 min before immersing them into a 1 g·L^{-1} aqueous solution of polyethyleneimine (PEI, hyperbranched, M_W ~25,000 g·mol^{-1} LS, Sigma-Aldrich, Merck, Darmstadt, Germany) for 30 min. Excess PEI was removed by carefully dipping the electrochemical balance probes several times into MilliQ water.

Cantilevers were driven to oscillation using the additional photothermal laser [56]. The system was operated using the picobalance software (v1.2.6.0, Nanosurf AG, Liestal, Switzerland) and the CX control software (v3.10.5.14, Nanosurf AG, Liestal, Switzerland). Frequency sweeps in liquid were acquired before and after picking up single microspheres from a glass slide (11 mm x 11 mm x 1 mm) glued to the glass bottom disc to compensate for the additional height of the contact wire on the cantilever chip of the electrochemical balance probe. In order to attach the mass, the EBP was aligned above a particle and then approached. Surface forces, such as van der Waals, solvent exclusion, and electrostatic forces held the particles on the EBP when retracting it from the surface. Attached particles could be removed by crossing the liquid-air interface. The successful removal of the attached particles was

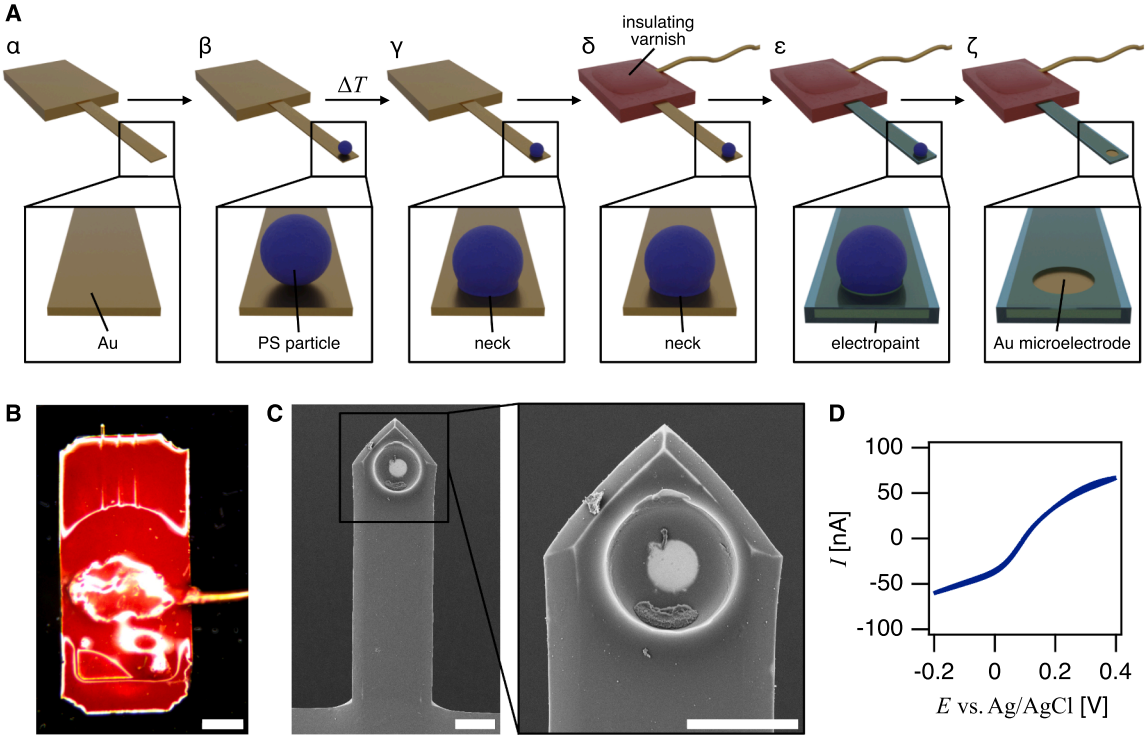

Fig. 1. Fabrication and characterization of electrochemical balance probes. A Electrochemical balance probes (EBPs) were fabricated based on commercial tipless AFM cantilevers. (α) An Au-coated tipless cantilever formed the foundation for the EBPs. (β) A polystyrene (PS) microsphere was placed on the free end of an AFM cantilever. (γ) Both were tempered at 200 °C for 180 s to form an increased contact area. (δ) A polyimide-insulated Ag-wire was attached to the cantilever chip to provide electrical contact. The electrical contact and the carrier chip were insulated with a red insulating varnish. (ε) The cantilever arm was coated with a cathodic electropaint for insulation. This process has been repeated several times to achieve better insulation. (ζ) The sacrificial PS particle has been removed with a micromanipulator to expose the previously masked area on the Au-electrode. Thereby, a planar-circular microelectrode has been created at the free end of the insulated cantilever. **B** Overview of the insulated cantilever with the planar Au-electrode area at its free end, the connection cable, and the insulation painted over the carrier chip. The scalebar represents 500 µm. **C** SEM image of an insulated cantilever and a zoom-in on the microelectrode area of an EBP. Scale bars are 20 µm. **D** Cyclic voltammogram of the microelectrode on the EBP in an aqueous hexacyanoferrate solution (5 mM/5 mM $K_4/K_3[Fe(CN)_6]$ in 100 mM KNO_3) at 50 mV·s^{-1}.

verified once the resonance frequency returned to its initial value and corroborated by optical microscopy. The phase sweeps were fit to equation Eq. (2) to extract the resonance frequency of the cantilever without f_N and with an attached mass $f_N(M)$. The actual size of the microspheres and their respective position on the cantilever were evaluated from optical microscopy images. The apparent mass M was calculated using Eq. (5) and was corrected for the position following Eq. (6) to obtain the actual particle mass m_{PB}.

2.4. Electrochemical picobalance

The electrochemical picobalance setup has been implemented into the Drive AFM setup described above. A photograph of the entire setup and key components is available in the supplementary materials (S1, cf. Fig. S1). Using the CX control software (v3.10.5.14, Nanosurf AG, Liestal, Switzerland) in user mode allowed to externally operate the photothermal excitation using an additional lock-in amplifier (MFLI 500 kHz, Zürich Instruments, Zürich, Switzerland) in phase-locked loop (PLL) mode. The excitation amplitude was fixed at 500 mV, which resulted in an oscillation amplitude of 3–5 nm. The PLL adjusted the excitation frequency to maintain a constant phase shift of 90° between the excitation and the response of the resonator. The shift in the cantilever's resonance frequency, $\Delta f_{N,}$ was monitored to trace the mass evolution over time. No effects due to swelling or degradation of the electropaint coating of the EBP have been observed.

Here, the integrated electrode on the EBPs acted as the working electrode in a three-electrode setup, and the applied potential was controlled using a CHi 750 E bipotentiostat (CH Instruments, Austin, USA). A coiled platinum wire (0.1 mm, 99.99 %, Goodfellow, Huntingdon, United Kingdom) acting as a counter electrode (CE) and a chlorinated wire as a pseudo reference electrode (pseudo-RE) were placed in a circular manner into the fluid cell around the position of the electrochemical balance probes acting as WE. The pseudo-RE was fabricated by electrochemically depositing AgCl onto a partially insulated Ag-wire (0.25 mm, PTFE insulated, Advent Research Materials, Oxford, United Kingdom) using an automated chlorider (ACl-01, npi electronic, Tamm, Germany). The offset of the pseudo-RE was verified against a commercial Ag/AgCl electrode (RE-5B, 3 M NaCl, BASi, West Lafayette, USA).

All signals from the lock-in amplifier (frequency shift, amplitude, phase) and the potentiostat (potential, current) were captured simultaneously using a low noise data acquisition system (Axon Digidata 1550 B, Axon Instruments, Molecular Devices, San Jose, USA) with a common time stamp. The data were verified using the raw data from the potentiostat for data analysis.

2.5. Cu deposition traced by the electrochemical picobalance

Copper was deposited electrochemically onto the µm-sized Au electrode at the free end of an electrochemical balance probe utilizing the three-electrode configuration inside the electrochemical picobalance setup specified above.

To avoid damage to the electrical insulation of the cantilevers, these home-build EBPs were fixated by paraffin wax (Paraplast, Sigma Aldrich, Merck, Darmstadt, Germany) to the cantilever holder rather than using any standard clamping mechanism. Moreover, the wax provided an additional insulating layer to the cantilever chip.

Before electrodeposition, each electrochemical balance probe was characterized by cyclic voltammetry (CV) in the range −0.2 V to +0.4 V vs. Ag/AgCl at a scan rate of 50 mV·s^{-1} in an electrochemical analyte solution containing 5 mM potassium hexacyanidoferrate(II) ($K_4[Fe(CN)_6]$, >98.5 %, Sigma-Aldrich, Darmstadt, Germany), 5 mM potassium hexacyanoferrate(III) ($K_3[Fe(CN)_6]$, >99.0 %, Sigma-Aldrich Darmstadt, Germany), and 100 mM potassium nitrate (>99.0 %, Carl-Roth, Karlsruhe, Germany) in MilliQ water. These CV experiments were performed in the electrochemical picobalance setup directly before Cu deposition. The analyte solution was replaced by MilliQ water thrice before exchanging the solution thrice for 10 mM H_2SO_4 (99.99 %, Sigma-Aldrich, Merck, Darmstadt, Germany). A reference experiment was conducted by applying −0.4 V vs. Ag/AgCl for 60 s with a potentiostat (CHi 750 E bipotentiostat, CH Instruments, Austin, USA) without any copper added to the supporting electrolyte solution. Then, the solution was exchanged for the electrolyte solution containing 3 mM $CuSO_4$ (99 %, Grüssing, Filsum, Germany) in 10 mM H_2SO_4 (99.99 %, Sigma-Aldrich, Merck, Darmstadt, Germany). During the copper electrodeposition, Cu^{II} was reduced to Cu^0 by applying $E_{red} = -0.4$ V vs. Ag/AgCl for 60 s with a potentiostat. The frequency shift, current, and potential were traced as specified above.

2.6. Data analysis for the electrochemical picobalance

The mass of the deposited copper was evaluated by two different methods: On one hand, based on the total charge transferred through the working electrode according to Faraday's law of electrolysis ($m_{faraday}$, Eqs. (10) and (11)) and on the other hand, by acquiring the frequency shift recorded by the AFM-based picobalance and evaluating it by purposely-written procedures in Igor Pro (v. 8.04 Wavemetrics, Portland, USA) (m_{PB}, Eqs. (5) and (6)). The position and dimension of the electrode on the cantilever were determined from SEM images by means of FiJi [57] using the free hand tool to outline the electrode area and the centroid function to determine the center of mass, i.e., the center of the electrode area (cf. Fig. S5). A similar approach was used previously to determine the location and center of mass of cells on AFM cantilevers for picobalance experiments [39,44,45,58]. The effective mass M was corrected for the mass position to calculate the actual deposited mass m_{PB} by Eq. (6).

2.7. Cu deposition in the electrochemical quartz crystal microbalance (EQCM)

Copper electrodeposition on macroscopic quartz sensors (5 MHz, 14 mm, Cr-Au, Quartz Pro, Jarfälla, Schweden) was conducted in a commercial quartz crystal microbalance (QCM) setup (QSense Explorer, Biolin Scientific, Göteborg, Schweden) equipped with a closed electrochemistry module (QEM401, Biolin Scientific, Göteborg, Schweden). In this setup, the QCM sensor acts as WE. The three-electrode configuration in the electrochemical QCM-cell was realized by a platinum sheet used as CE and an Ag/AgCl as RE (Dri-Ref 2SH, World Precision Instruments, Sarasota, USA). The QCM sensors were cleaned by immersing them into a 5:1:1 (v:v:v) mixture of MilliQ water, ammonia (25 w:v %, VWR International S. A. S, Rosny-sous-Bois, France), and hydrogen peroxide (30 w:v %, Fisher Scientific, Schwerte, Germany) at 75 °C for 5 min. Subsequently, the sensors were thoroughly rinsed with MilliQ water and dried in a stream of nitrogen. The offset of the RE was verified against a commercial RE (RE-5B, 3 M NaCl, BASi, West Lafayette, USA). For the copper deposition, −0.4 V vs. Ag/AgCl was applied to the QCM sensor WE for 60 s using a potentiostat (Zennium, Zahner-Elektrik, Kronach, Germany). Measurements were conducted in an aqueous solution containing 10 mM $CuSO_4$ (99 %, Grüssing, Filsum, Germany) and 10 mM H_2SO_4 (99.99 %, Sigma-Aldrich, Merck, Darmstadt, Germany) supporting electrolyte in a constant flow of 100 µL·min^{-1} facilitated by a peristaltic pump (IPC multichannel dispensing pump, ISMATEC, Cole-Parmer, Wertheim, Germany).

Frequency shifts were converted into mass shifts using the Sauerbrey equation (Eq. (12)): [19]. The third overtone was used for evaluation. However, comparable results were obtained for higher oscillation modes. The Faraday mass was determined similarly to the electrochemical picobalance according to Eq. (11).

2.8. Scanning electron microscopy images of electrochemical balance probes

We analyzed the EBPs by scanning electron microscopy (SEM) after sputter coating a thin layer of platinum ($d = 2$ nm) using a field emission SEM (Leo 1530, Zeiss, Oberkochen, Germany) operated at 3 kV acceleration voltage and a working distance of 8.1 mm with an ET detector.

3. Results and discussion

In the following, it is demonstrated how the AFM-based picobalance, which was initially developed to study small mass fluctuations in cells [39], was adapted to also follow small mass changes on µm-sized electrodes during dynamic electrochemical experiments. Faraday's law allowed for a direct correlation between deposited mass and simultaneously acquired current. However, an essential prerequisite for electrochemical experiments with the picobalance were fully insulated cantilevers with an integrated microelectrode.

3.1. Preparation of electrochemical balance probes

The preparation of suitable electrochemical probes is central for performing electrochemical experiments by AFM, such as scanning electrochemical microscopy [50,59,60], nanomanipulation [61], or direct force measurements [49,62,63]. Here, we adapted a template-assisted procedure originally developed to prepare electrochemical colloidal probes [49]. However, electrochemical probes for the picobalance have a highly defined electrode area at the end of the AFM cantilever as a primary requirement. Therefore, we opted for a simplified approach where a circular microelectrode was obtained by masking the later electrode area using a sacrificial particle and applying an insulating coating for the rest of the cantilever. The respective cantilevers will be denoted as electrochemical balance probes (EBPs) throughout this work, and Fig. 1 provides a comprehensive overview of the required preparation steps and the characterization of EBPs.

The individual steps of the manufacturing process are displayed in Fig. 1A (α-ζ). The electrochemical balance probes (EBPs) were fabricated based on commercial gold-coated conductive cantilevers (α). The future electrode area located at the free end of the EBP was masked by attaching a sacrificial polystyrene (PS) particle (β). Annealing the cantilever and PS bead above its glass transition temperature at 200 °C for 180 s generated an increased, approximately circular contact area (γ). Subsequently, the gold-coated cantilever chip was contacted with an insulated silver wire using conductive silver paint. This attachment point was additionally sealed by UV-curable glue to insulate the contact point and mechanically reinforce the attachment (δ). Moreover, the entire chip was electrically insulated using red insulating varnish (δ). The varnish was carefully dip-coated onto the chip using a micromanipulator, leaving only the lever arm uncoated. This lever arm was insulated using a commercial transparent cathodic electropaint [49,61,64–67], which was deposited under potentiostatic control (ε). Three coating cycles with intermediate heat annealing of the individual coating layers were performed to achieve a defect-free coating, especially at the edges of the lever arm. After completing these insulating steps, the sacrificial particle was removed mechanically by an etched wire mounted to a motorized micromanipulator. The removal of the particle resulted in a defined hole in the insulation that uncovered the underlying gold coating of the cantilever, which acted in the following as the microelectrode of the EBP (ζ). Fig. 1B shows an optical microscopy image illustrating the red insulation on the cantilever chip and the attached insulated wire. Fig. 1C shows the insulated cantilever arm and the integrated electrode of the EBP by scanning electron microscopy (SEM).

As we will demonstrate later, the multi-step insulation was essential to ensure that all faradaic currents originate only from the electrode area integrated into the fully insulated cantilever (cf. Fig. 1C, S2). The flexibility and transparency of the thin polymeric coating enabled photothermal excitation of the cantilever oscillation and facilitated the optical readout of the cantilever response while maintaining the required electrical insulation of the underlying gold coating of the cantilever. The coating did not show any signs of wear or swelling, and also seems to be resistant to the IR laser illumination. In contrast, a thicker and opaque insulation layer could be applied to the cantilever chip, also providing mechanical stability to the attachment point of the wire.

3.2. Electrochemical characterization of the electrodes for the picobalance

Cyclic voltammetry (CV) provides a direct approach for characterizing the performance of probes for electrochemical AFM [60,62,63,68,69]. Commonly, redox couples, such as ruthenium complexes or hexacyanoferrate, are used for CV of nm- or µm-sized electrodes on AFM cantilevers [60,68]. Here, we characterized the electrode properties of the EBPs by CV with the redox couple 5 mM $K_4[Fe(CN)_6]$ and 5 mM $K_3[Fe(CN)_6]$ in 100 mM KNO_3 as supporting electrolyte [49,60,70]. The CVs with the EBP as a working electrode were acquired at 50 mVs^{-1} between −0.2 V and +0.4 V vs. Ag/AgCl in a three-electrode setup incorporated into a commercial AFM fluid cell [49,61].

Fig. 1D shows a typical CV acquired with an EBP, which was mounted inside the same electrochemical cell that was also part of our picobalance setup (cf. Fig. 2 and Fig. S1). The shape of the acquired CV matched the one typically observed for microelectrodes or ultramicroelectrodes: No pronounced oxidation or reduction peaks and overlap of both scan directions [1,71]. The limiting currents were in the order of 50 nA for this EBP, which is compatible with a microelectrode area of 533 μm^2, corresponding to a circular diameter of ~26 µm (cf. also supplementary materials for an SEM image of this EBP). The CV shown in Fig. 1D was acquired with an EBP, which has been insulated by three repetition cycles of electropaint coating. For lever arms, which were less insulated, higher currents have been observed (supplementary materials S2, Fig. S2), indicating that faradic currents from the edges of the lever arm were involved.

3.3. Setup of the electrochemical picobalance

Fig. 2 shows a schematic representation of the picobalance setup used in this study. A photograph of the setup is available in the supplementary materials (S1, Fig. S1). The electrochemical cell was integrated into the AFM-based setup. The design of the electrochemical cell was analogous to those previously described [49,61]. For the picobalance experiments, the EBP acted as the working electrode (WE), the counter electrode (CE) was a coiled Pt-wire, and the reference electrode (RE) was a chlorinated silver wire (Ag/AgCl pseudo-RE). The mass-sensing part of the picobalance was based on a commercial AFM with additional photothermal excitation of the cantilever [44,46]. Other groups have also used a similar setup to implement AFM-based picobalances [39,40,44–46].

The general working principle of the picobalance is based on determining the frequency shift of an oscillating cantilever, which is driven near its resonance frequency f_N [39]. Here, the EBP was driven by an intensity-modulated laser diode that locally heats the cantilever close to its clamped end at the carrier chip [56]. The resulting EBP oscillation was detected by a second laser, which is reflected on the free end of the EBP to a position-sensitive photodiode according to the optical light-lever technique [43]. The frequency and phase of the readout signal were analyzed via a lock-in amplifier and correlated to the input signal modulating the excitation laser. A phase-locked loop (PLL) maintained a constant phase of 90° with respect to the excitation signal by continuously adjusting the excitation frequency. The corresponding frequency shift Δf_N was acquired and converted to a mass change as outlined below.

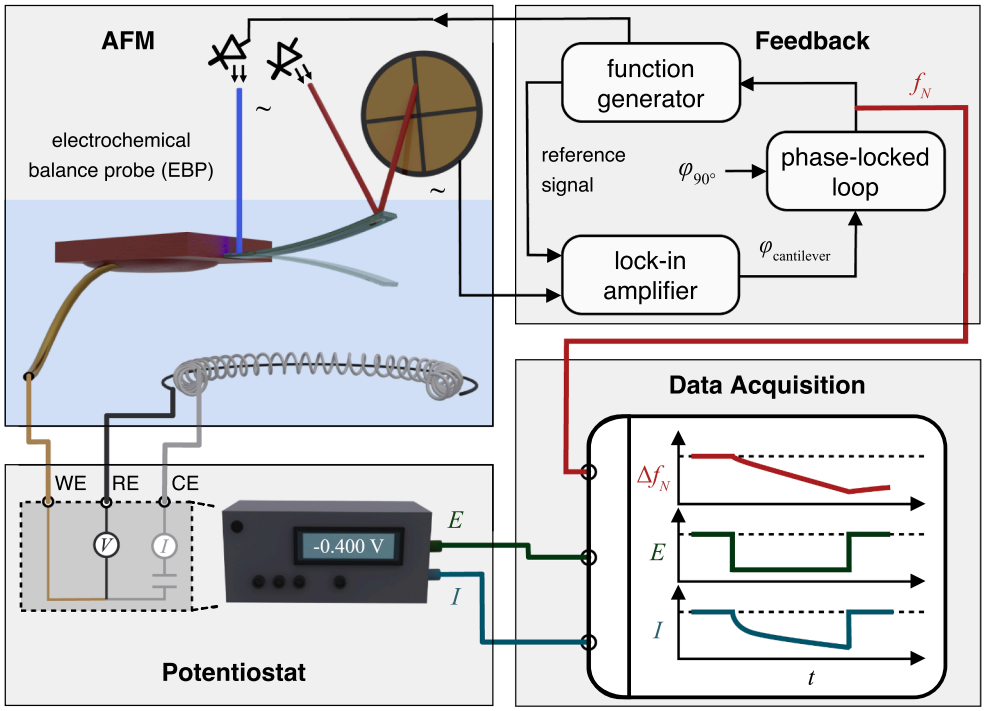

Fig. 2. Schematic representation of the electrochemical picobalance setup. The central part of the setup was the custom-made electrochemical balance probe (EBP) based on a commercial, conductive AFM cantilever. The EBP was mounted in an AFM equipped with two separate lasers: an intensity-modulated laser, which drives the cantilever to oscillation close to its clamped end, and a readout laser reflected at the cantilever's free end to a position-sensitive photodiode. A function generator controlled the photothermal excitation. The lock-in amplifier analyzes the frequency and phase of the photodiode signal. A phase-locked loop (PLL) maintains a constant phase shift of 90° between the cantilever oscillation and the excitation by adjusting the excitation frequency. The EBP acted not only as a mass sensor but also as the working electrode controlled by a potentiostat. The coiled Pt wire (CE) and chlorinated Ag-wire were implemented into the fluid cell of the AFM to complete a three-electrode electrochemical cell. All data signals from the picobalance and the potentiostat were acquired with a common time stamp.

3.4. *Theory of mass sensing by the picobalance*

Commonly, the oscillation of an AFM-cantilever can be described in a first-order approximation as a driven underdamped oscillator [72,73]. The oscillation is defined by the frequency f at which the oscillator is driven, the resonance frequency f_N, and the quality factor $\widetilde{Q_f} > 1$. The oscillation amplitude A as a function of the resonator's frequency can described according to [72,73]

$$A(f) = \frac{a\, {f_N}^2}{\sqrt{\left(f_N^2 - f^2\right)^2 + \left(\frac{f_N f}{\widetilde{Q_f}}\right)^2}} + a_1 f + a_2 \tag{1}$$

with a accounting for the amplitude of the excitation. The parameters a_1 and a_2 represent a description for a linear background due to the frequency dependent excitation efficiency and amplitude noise. The phase shift φ of a driven and damped harmonic oscillator is given by

$$\varphi(f) = \tan^{-1}\left(\frac{\widetilde{Q_f}\left(f_N^2 - f^2\right)}{f_N f}\right) + b_1 f + b_2 \tag{2}$$

where b_1 accounts for phase lags of photothermal excitation and electronics and b_2 is related to phase contributions of higher modes [72,73].

Generally, the resonance frequency f_N of a harmonic oscillator can be expressed by its effective mass m^* and its spring constant k:

$$f_N = \frac{1}{2\pi}\sqrt{\frac{k}{m^*}} \tag{3}$$

After attaching an additional mass M, e.g. a colloidal particle, f_N is shifted to a lower frequency $f_N(M)$ as the effective mass changes to $m^* + M$:

$$f_N(M) = \frac{1}{2\pi}\sqrt{\frac{k}{m^* + M}} \tag{4}$$

Fig. 3 summarizes the resulting changes in the amplitude $A(f)$ and the phase spectrum $\varphi(f)$ upon attachment of an additional mass, i.e., a tungsten microsphere with a diameter of 12.7 µm. The attached mass M can in principle be directly calculated according to Eq. (5) based on the frequency shift $\Delta f_N = f_N - f_N(M)$:

$$M = \frac{k}{4\pi^2}\left[\frac{1}{(f_N - \Delta f_N)^2} - \frac{1}{f_N}\right] \tag{5}$$

However, Eq. (5) assumes that the mass is attached exactly at the free end of the cantilever, which is normally not the case [39,40,45]. The apparent mass depends on the position x_c of the mass M on the cantilever with a length L and the mode of oscillation (supplementary materials S3). Here, only the first mode has been excited and was considered in the data evaluation. A correction factor based on the oscillation amplitude $\psi(x)$ is needed to relate the apparent mass M to the actual mass m_{PB} (supplementary materials S3, Fig. S4):

$$m_{PB} = M\frac{1}{\psi(x_c)^2} \tag{6}$$

For a rectangular beam of the length L, the first oscillation mode can be described by

$$\psi(x) = \alpha\left[\sin(\xi x) - \sinh(\xi x) + \frac{(\sin(\xi L) + \sinh(\xi L))(\cosh(\xi x) - \cos(\xi x))}{\cos(\xi L) + \cosh(\xi L)}\right] \tag{7}$$

with a normalization constant α to fulfill condition $\psi(L)^2 \stackrel{!}{=} 1$. ξ is related to the cantilever length by

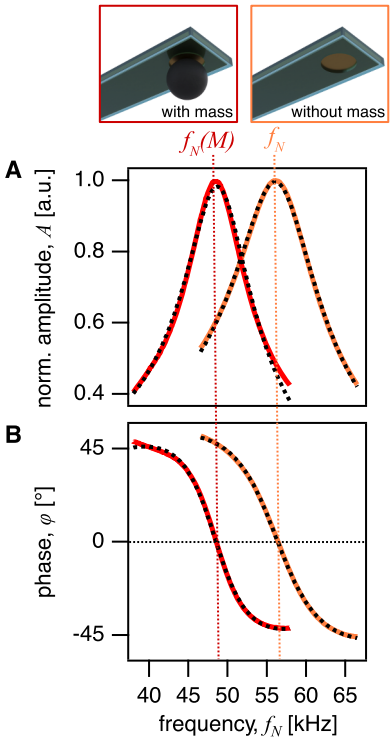

Fig. 3. Mass sensing with an electrochemical balance probe. A Normalized amplitude A and **B** phase φ spectra of an EBP without and with a tungsten microsphere ($d = 12.7$ µm) as an external load. Amplitude and phase have been fitted to eqns. (1) and (2) (dashed lines).

$$\cos(\xi L)\cosh(\xi L) + 1 = 0. \tag{8}$$

3.5. Added mass as static calibration of electrochemical balance probes

The added mass method, which is based on Eqs. (4) and (5), is widely used to calibrate spring constants of AFM cantilevers [54]. In this method, small, µm-sized, colloidal particles from high-density materials, such as gold or tungsten, are attached by capillary forces to the free end of an AFM-cantilever [54,74]. The resulting frequency shift is related to the theoretical mass based on the top-view dimensions of the microsphere. However, it has been demonstrated that additional layers on the lever arm can impact the mechanical properties of cantilevers [75,76]. The EBPs comprise a rather complex sandwich structure with a silicon core, enclosed by an adhesive Cr interlayer, the conductive gold coating, wrapped by the insulating electropaint layer. Consequently, we had to verify that mass sensing was possible for these non-standard probes using the added mass method. These experiments were performed in liquid, here 0.1 mM HCl and pH 4, in order to emulate the environmental conditions encountered during the electrochemical experiments. Moreover, the EBPs were driven photothermally, generating much clearer resonance peaks with higher amplitudes and quality factors than piezoelectric or thermal excitation [42].

By evaluating the resonance frequency f_N, the experimental mass m_{PB} was calculated according to Eq. (5) and (6). This mass was compared to the theoretical mass m_{theo} Eq. (9) as determined by the optical dimensions and the position of the respective particles on the cantilever.

$$m_{theo} = \frac{4}{3}\pi\left(\frac{d}{2}\right)^3 \rho \tag{9}$$

We utilized tungsten microspheres of various sizes as externally attached masses M for these experiments. The theoretical mass m_{theo} was calculated from the volume V and the density ρ (Eq. (9)). The volume was determined from the particle diameter d as measured by optical microscopy. Moreover, the position of the particles on the lever arm of the EBPs has been considered according to Eq. (6). The correction factor for an EBP depending on the location of the added mass is shown Fig. S4B in the supplementary materials. The position x_c was determined by allocating the particle's location via optical microscopy. A similar approach has been utilized previously for localizing cells in gravimetric studies by picobalance [39,40,44,45,77].

Fig. 4 summarizes the experimental results for weighing 10 individual tungsten microspheres of various sizes (6.8 µm < d < 13.3 µm) in the picobalance with an EBP. The respective theoretical masses m_{theo}, as determined by the radius and density, ranged thus between 2.1 ng and 20 ng. These masses m_{theo} have been compared to the ones determined by the picobalance m_{PB}. Ideally, one expects a ratio $m_{PB}/m_{theo} = 1$ as indicated by the dashed line in Fig. 4. The error bars shown were determined by error propagation based on the uncertainty of the spring constant calibration for the cantilever with which m_{PB} has been determined and the inaccuracy of the diameter obtained by optical microscopy for the theoretical mass m_{theo}. The good agreement for all added masses, which scattered around the dashed line representing perfect agreement, demonstrated that despite their complex structure, the ECBs were capable of quantitative mass determination in the nanogram regime.

3.6. The electrochemical picobalance

The electrodeposition of copper on metal electrodes accounts for one of the most fundamental and best-studied processes in electrochemistry [78]. Here, we examined the deposition of Cu on the µm-sized Au-electrode (cf. Fig. 1C and Fig. S5) of an EBP in combination with the AFM-based picobalance (cf. Fig. 2). The electron transfer and resulting Cu deposition have been followed simultaneously by the frequency shift $\Delta f_N(t)$ and the faradaic current $I(t)$. For comparison, we performed the experiment under analogous conditions on a macroscopic Au-electrode using the QCM-D technique. A reductive potential of $E_{red} = -0.4$ V vs. Ag/AgCl was applied to the Au-electrode for both setups. The deposition was carried out in 3 mM $CuSO_4$ (10 mM for the EQCM experiments) with 10 mM H_2SO_4 as a supporting electrolyte. These experimental conditions fall within the standard conditions reported in the literature for Cu deposition [29,31]. The electrochemical reduction of Cu^{II} at the EBP microelectrode leads to a deposition of solid Cu^0 on the electrode. According to Faraday's law of electrolysis, the faradaic mass $m_{faraday}$ should equal the mass m_{PB} sensed by the picobalance (Eq. (6)).

Fig. 5A shows the frequency shift Δf_N, current I, charge Q, and potential E during the electrodeposition of Cu on an EBP as determined by the electrochemical picobalance when E_{red} was applied via the

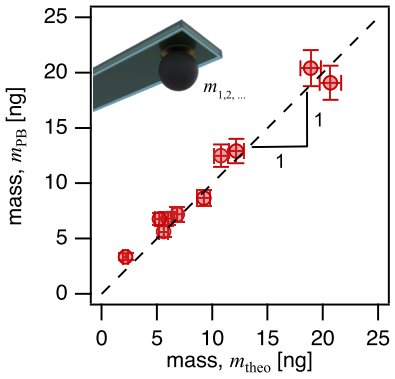

Fig. 4. Added mass method for electrochemical balance probes. Comparison between the masses of tungsten microparticles of different sizes as determined by their top view dimensions (m_{theo}) and as determined by the resonance shift of an electrochemical balance probe (m_{PB}) as determined by the AFM-based picobalance. The dashed line represents a slope of 1, which means ideal correspondence between the two methods.

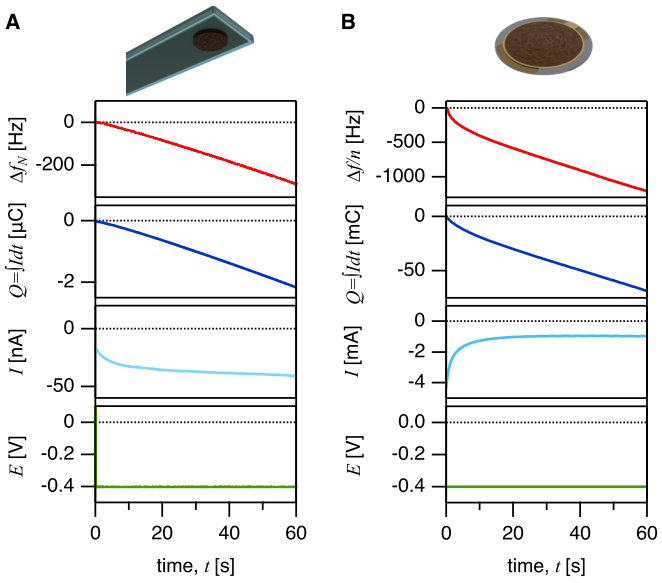

Fig. 5. Cu electrodeposition on an electrochemical balance probe and a QCM sensor. A Frequency shift Δf_N, total charge $Q = \int I\, dt$, current I and potential E during electrochemical deposition of Cu on an EBP microelectrode in 3 mM $CuSO_4$ and 10 mM H_2SO_4 at −0.4 V for 60 s as detected by the electrochemical picobalance. **B** Frequency shift $\Delta f/n$, total charge $Q = \int I\, dt$, current I and potential E during electrochemical deposition of Cu on an Au-coated QCM sensor in 10 mM $CuSO_4$ and 10 mM H_2SO_4 at −0.4 V for 60 s. EQCM data is shown for the 3rd overtone. The onset of the potential was set to $t = 0$ for both types of sensors. Note the different axis scaling for the EBP microelectrode and the macroscopic QCM sensor due to the large differences in electrode size.

potentiostat. A negative frequency shift of up to −288 Hz after 60 s corresponded to a mass deposition on the microelectrode of the EBP. By contrast, no change in frequency could be detected when E_{red} was applied in pure supporting electrolyte only, i.e., without Cu in the measurement solution (supplementary materials S4, Fig. S6). Hence, the frequency shift can be assigned to the electrodeposition of copper and was not resulting from the electromechanical stress on the cantilever as it had been observed in some conditions for cantilevers with Au-coating [79–81]. After 5–10 s, the deposition current I was constantly ~40 nA. The corresponding total charge $Q(t)$ was determined by integrating the current $I(t)$:

$$Q(t) = \int_0^t I(t)dt \tag{10}$$

We conducted an analogous electrodeposition of Cu on macroscopic Au-coated QCM sensors ($A = 1.13\ cm^2$) in an EQCM (cf. Fig. 4B). Again, a continuous negative frequency shift $\Delta f/n$ was observed when a reductive potential of $E_{red} = -0.4$ V vs. Ag/AgCl was applied for 60 s to induce the copper deposition. The frequency shift is normalized to the overtone n, and data for the 3rd overtone are shown. The maximum shift was ~−1200 Hz after 60 s. In contrast to the EBP, the currents were significantly higher, about 1 mA, due to the larger electrode area. However, a direct correlation between the frequency response Δf_N (or $\Delta f/n$) and transferred charge Q at the electrode became evident for both methods.

3.7. Correlation between electrochemical and gravimetric mass

Faraday's law of electrolysis states that the amount of an electrochemical reaction product is proportional to the charge Q transferred through the electrolyte/electrode interface [1,3]. Hence, the mass of a reactant deposited by an electrochemical reaction is given by

$$m_{\text{faraday}} = -\frac{QM_W}{zF} \tag{11}$$

where z is the number of electrons transferred to form one mole of the reactive species with the molecular weight M_W, and F is the faraday constant [1]. Faraday used gravimetric determination of m_{faraday} in his original experiments. Faraday's law can be directly applied to the electrodeposition of Cu on the EBP microelectrode and the faradaic mass m_{faraday} (Eq. (11)) must equal the mass sensed by the picobalance m_{PB} (Eq. (6)). This relation has also been used extensively to characterize EQCM sensors and determine their mass sensitivity [30–32].

Here, we performed additional experiments by EQCM under identical conditions as a benchmark. The mass from EQCM data was evaluated by the Sauerbrey equation [19] which relates the frequency shift Δf_{EQCM} normalized to the overtone n to a mass per unit area m_{EQCM}/A via a sensitivity constant C of the quartz sensor.

$$m_{\text{EQCM}}\Big/A = -C\frac{\Delta f_{\text{EQCM}}}{n} \text{ with } C = \frac{2f_0}{A\sqrt{\rho\mu}} \tag{12}$$

The sensitivity constant $C = 17.7\ \text{ng cm}^{-2}\ \text{Hz}^{-1}$ is determined by the fundamental resonance frequency f_0, the area A of the electrode, the sensor's density ρ, and its shear modulus μ. Since the deposited Cu layer is thin and rigid, the Sauerbrey equation could be applied here without any corrections or viscoelastic modeling [20].

Fig. 6 summarizes the deposited mass versus time as determined gravimetrically by the electrochemical picobalance and the EQCM, respectively, and electrochemically by Faraday's law. To compare the results obtained by both techniques, the deposited masses have been normalized to the electrode areas of the respective sensors. The electrode area of the EBP was determined from SEM images after the deposition (supplementary materials S3, Fig. S5). It should be noted that the areas of the two electrodes vary by several orders of magnitude (533 μm^2 versus 1.13 cm^2). The normalized gravimetric masses agreed well with the masses determined according to Faraday's law of electrolysis for both techniques. Interestingly, the deviation between electrochemically determined mass and the gravimetric one is higher for the EQCM. We attribute this to a higher surface area due to the electrode's roughness (supplementary materials S5, Fig. S7). This type of effect has been reported previously for copper deposition on polycrystalline gold [31, 32,82]. Moreover, roughness is generally known to impact QCM measurements in liquid [83].

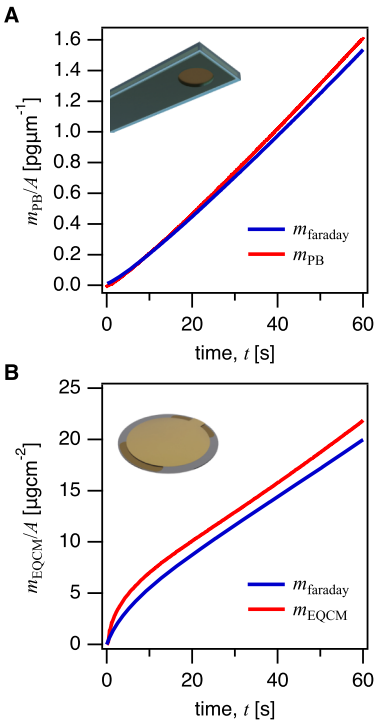

Fig. 6. Deposited copper mass as determined by electrochemical picobalance, EQCM, and Faraday's law. Mass of Cu deposited electrochemically on the microelectrode of the EBP as determined from the frequency shift in the picobalance (m_{PB}) and by integration of the current according to Faraday's law ($m_{faraday}$). **B** Mass of Cu deposited on an Au-coated quartz-crystal in an EQCM as determined from the Sauerbrey equation (m_{EQCM}) and Faraday's law ($m_{faraday}$). For both experiments, a potential of −0.4 V (vs. Ag/AgCl) was applied for 60 s. The faradaic ($m_{faraday}$), and gravimetric masses (m_{PB}, m_{EQCM}) have been normalized to the electrode areas (533 μm^2 vs. 1.13 cm^2).

3.8. Mass sensitivity of the electrochemical picobalance

The mass change determined by the two methods, i.e., gravimetrically and electrochemically, was in excellent agreement not only for the EQCM but in particular also for the AFM-based picobalance. Figs. 5 and 6 corroborate that the picobalance can be utilized in an electrochemical mode. In the following, we will address the question of the detection limitations of the electrochemical picobalance. The combination of the picobalance with electrochemistry allows addressing the mass sensitivity and mass resolution of the picobalance technique in a new way: Electrodeposition allows for a defined mass deposition over time, in contrast to adding masses like the tungsten beads in section 3.5 or small blocks of silicon [39]. Moreover, the deposited mass could be verified independently of optical or electron microscopy resolution by means of Faraday's law. In the following, we concentrate on the so-called mass-sensitivity [40,84,85].

The resolution of the electrochemical channel of the picobalance depends strongly on the electrochemical performance of the EBPs (details in the supplementary materials, S2, and S6). Accurate mass determination by Faraday's law requires optimal electrical insulation of the probes. Any defects in the insulation will lead to additional electrochemically active areas, which would lead to additional deposited masses outside the intended electrode area (supplementary materials S2, Fig. S3). The chip could be coated with relatively thick layers of non-transparent insulating varnish. Moreover, mounting EBPs via paraffin provided additional mechanical stability and electrical insulation of the contact point between the chip and the wire. In consequence, we found that the quality of the electropaint insulation on the lever arm was crucial. Due to the small microelectrode area, even minor defects on the lever arm disturbed the mass evaluation drastically. The electrochemical response of the EBPs varied with the number of layers of electropaint. This variation could also be traced in the CVs, where with an increasing number of layers, the overall current reduced significantly. Corresponding CVs are available in the (S2, Fig. S2). After three layers, the current density in the CVs did practically not change. Hence, we decided on 3 layers for all results presented in this study. For only one and two layers of electropaint, the coating did show imperfections, especially at the edges. Defects in the insulation became evident after electrodeposition and could be visualized (supplementary materials, S2, Fig. S2).

By contrast, the gravimetric mass resolution depended primarily on the choice of the cantilever (cf. Fig. S8) and the accuracy with which the spring constant of the EBP could be determined according to Eqs. (4) and (5), respectively. Due to the more complex structure of the EBPs, approaches that are based on geometrical dimensions and homogeneous material constants (e.g. [76]). will most likely not provide sufficiently accurate results. The thermal noise method [86] and added mass method [54] are more appropriate for the EBPs, as these methods are based directly on the resonator properties.

Combining the picobalance with electrochemistry allowed dynamic mass deposition on the picobalance for the first time. So far, the picobalance has been only tested by static loads, i.e., colloidal particles of defined mass (cf. section 3.4) that have been attached to the cantilever [39,40]. It should be kept in mind that the AFM-based picobalance was originally developed for following small mass changes in living cells. The linear increase of mass with time during Cu-deposition allowed for a dynamic approach for which the mass could be determined independently according to Faraday's law (cf. Fig. 6). For the picobalance, the absolute mass of Cu electrodeposited was 705 pg after 60 s with a resolution of 2.44 pg·Hz^{-1}, which demonstrated that mass changes < 1 pg can be readily detected by the picobalance (supplementary materials S6, Fig. S9). The sensitivity has been extracted from the slope of a mass vs. frequency shift plot shown in Fig. 7. For QCM and EQCM, the mass sensitivity is normally stated per unit area of the sensor [87]. Hence, for the electrochemical picobalance, we found an 'area normalized' mass sensitivity of approximately 4.6 fg·μm^{-2}·Hz^{-1} (or 460 ng·cm^{-2}·Hz^{-1}) following the QCM convention. By comparison, we determined a sensitivity of 17.5 ng·cm^{-2}·Hz^{-1} for the commercial QCM resonator, which is in good agreement with 17.7 ng·cm^{-2}·Hz^{-1} as stated by the manufacturer [87]. As the electrode of the EQCM is much larger than the one on the cantilever (533 μm^2 vs. 1.13 cm^2), we find that the mass sensitivity normalized to the electrode area is favorable for the EQCM. On the other hand, it should be kept in mind that on an absolute scale, the picobalance can detect significantly smaller absolute mass changes supplementary materials S6, Fig. S9C). The difference between the two techniques becomes especially evident for small frequency shifts (cf. insets in Fig. 7).

4. Conclusions

In this feasibility study, we presented the combination of electrochemistry with an AFM-based picobalance (electrochemical picobalance), for the first time. The electrodeposition of Cu allowed for dynamic calibration of the picobalance as the deposited mass increased strictly linearly with time and could additionally be determined in an independent manner via the Faradaic current. While the mass sensitivity of the electrochemical picobalance is smaller than for the EQCM, it is able to determine mass changes for absolute masses several orders smaller than the EQCM. If one aims for the study of single-entity electrochemical effects, such as for cells, this absolute sensitivity will be advantageous and could be determined here for the first time by a combination of two independent techniques. In contrast, for homogenous electroactive films, the EQCM might be the better choice, provided that these films do not require special hydrodynamic data treatment. With the experimental setup used here, we could confirm that mass changes of 1 pg could be resolved by the electrochemical picobalance. With some experimental improvements, e.g., the cantilever used (cf.

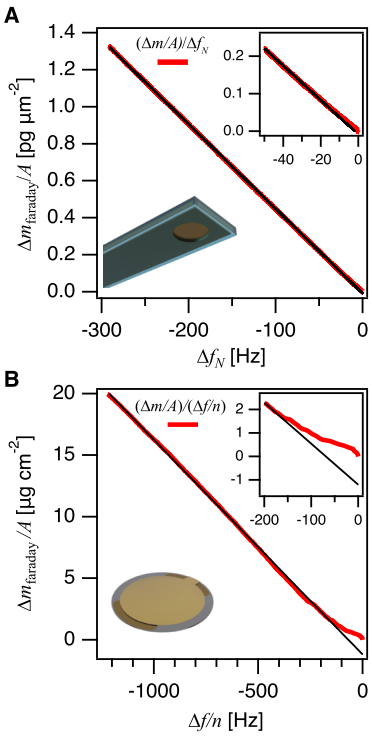

Fig. 7. Mass sensitivity of the electrochemical picobalance and EQCM. A Mass sensitivity for the electrochemical picobalance extracted from the frequency change rate with the added Faraday mass $m_{faraday}$. **B** Mass sensitivity for the EQCM setup was determined in an analogous manner. The insets show the initial deposition at short deposition times and, thus, small frequency shifts.

supplementary materials S6, Fig. S8), and the digital resolution of AD converters, even higher mass resolutions seem feasible.

In the future, the combination of electrochemistry and the picobalance will provide alternative approaches to some electrochemical problems, especially in relation to soft matter. The hydrodynamic damping of extended polymeric films on QCM provides a number of challenges to determine the bound mass. In particular, probing the kinetics for electropolymerization and electrogelation is not straightforward for thicker films. In contrast to the EQCM, the electrochemcial picobalance is not based on shear oscillations; hence, the hydrodynamic damping takes place by the vertical oscillation of the cantilever. Microcantilevers have been used in the past to successfully trace viscosity and mass density for bulk polymerizations in small volumes [72]. The electrochemical picobalance fosters direct electropolymerization on the mass sensor, i.e., the EBP microelectrode. Hence, this technique provides a complementary approach to studying the polymerization at interfaces.

So far, the picobalance has been primarily applied to monitor mass changes in living cells [39,40,44–46]. Addressing the mass changes of single cells upon external stimuli under various time scales represents an important tool for cell biology, and the here-presented setup can extend this approach to the cellular bioelectric state [52,88]. The bioelectrochemical stimuli for the cell are supposed to have an influence on the cell metabolism [51]. With the implementation of the electrochemical picobalance, bioelectrical stimuli to cells and the resulting mass changes can be studied with unprecedented accuracy. The option of such studies should receive considerable interest [52]. It has also been shown that electrical stimulation can impact cell proliferation, signaling pathways, and immunomodulation [89–91]. So far, this relation has been studied primarily via volume changes and optical microscopy. However, the mass determination by the picobalance has the potential to provide a much higher mass and time resolution than previous approaches. It should be pointed out that these studies would not be limited to eukaryotic cells but could also be applied to, for example, bacteria [92].

CRediT authorship contribution statement

Nadine Raßmann: Writing – original draft, Visualization, Investigation, Formal analysis, Data curation, Conceptualization. **Roman E. J. Glaß:** Data curation, Investigation, Writing – review & editing. **Nicolas Helfricht:** Writing – review & editing, Supervision, Conceptualization. **Georg Papastavrou:** Writing – review & editing, Writing – original draft, Supervision, Funding acquisition, Conceptualization.

Declaration of competing interest

The authors declare the following financial interests/personal relationships which may be considered as potential competing interests: Georg Papastavrou reports equipment, drugs, or supplies was provided by Nanosurf AG. If there are other authors, they declare that they have no known competing financial interests or personal relationships that could have appeared to influence the work reported in this paper.

Acknowledgments

The authors gratefully acknowledge the help of Nina Volk, Sebastian Sittl, and the Keylab for Electron Microscopy of the Bavarian Polymer Institute with SEM imaging of the EBPs. Moreover, the authors thank LVH Coatings for the generous gift of the ClearClad electropaint. The authors thank the Nanosurf AG (Liestal Switzerland) and, in particular, Gotthold Fläschner (Nanosurf AG) for fruitful discussions on the picobalance during the initial stage of the project. Nadine Raßmann acknowledges financial support through a Kekulé stipend granted by the Fonds of the Chemical Industry.

The research was funded by the German Science Foundation (DFG) within the collaborative research center “Multitrans” (Project number 492723217 (CRC 1585), subproject C03).

Supplementary materials

Supplementary material associated with this article can be found, in the online version, at doi:10.1016/j.electacta.2025.146907.

Data availability

Data will be made available on request.

References

[1] A.J. Bard, L.R. Faulkner, H.S. White, Electrochemical Methods: Fundamentals and Applications, John Wiley & Sons, 2022.
[2] N. Eliaz, E. Gileadi, Physical Electrochemistry: Fundamentals, Techniques, and Applications, John Wiley & Sons, 2019.
[3] M. Faraday, Experimental researches in electricity. Seventh series, Phil. Trans. R. Soc. 124 (1834) 77–122, https://doi.org/10.1098/rstl.1834.0008.
[4] A.R. Hillman, The EQCM: electrogravimetry with a light touch, J. Solid. State Electrochem. 15 (7–8) (2011) 1647–1660, https://doi.org/10.1007/s10008-011-1371-2.
[5] L. Broch, L. Johann, N. Stein, A. Zimmer, R. Beck, Real time in situ ellipsometric and gravimetric monitoring for electrochemistry experiments, Rev. Sci. Instrum. 78 (6) (2007) 064101, https://doi.org/10.1063/1.2743273.
[6] M. Biermann, C. Leppin, A. Langhoff, T. Ziemer, C. Rembe, D. Johannsmann, An electrochemical quartz crystal microbalance (EQCM) based on microelectrode arrays allows to distinguish between adsorption and electrodeposition, Analyst 149 (7) (2024) 2138–2146, https://doi.org/10.1039/d3an02210b.
[7] A. Cuenca, J. Agrisuelas, J.J. García-Jareño, F. Vicente, Alternating current electrogravimetry of copper electrodissolution in a sulfuric acid solution, Electrochim. Acta 235 (2017) 374–383, https://doi.org/10.1016/j.electacta.2017.03.079.
[8] M.K. Nisiewicz, A. Gajda, A. Kowalczyk, A. Cupriak, A. Kasprzak, M. Bamburowicz-Klimkowska, I.P. Grudzinski, A.M. Nowicka, Novel electrogravimetric biosensors for the ultrasensitive detection of plasma matrix metalloproteinase-2 considered a potential tumor biomarker, Anal. Chim. Acta 1191 (2022) 339290, https://doi.org/10.1016/j.aca.2021.339290.

[9] V. Vanoppen, D. Johannsmann, X. Hou, J. Sjölund, P. Broqvist, E.J. Berg, Exploring metal electroplating for energy storage by quartz crystal microbalance: a review, Adv. Sens Res. 3 (9) (2024), https://doi.org/10.1002/adsr.202400025.
[10] P. Lemaire, T. Dargon, D. Alves Dalla Corte, O. Sel, H. Perrot, J.M. Tarascon, Making advanced electrogravimetry as an affordable analytical tool for battery interface characterization, Anal. Chem. 92 (20) (2020) 13803–13812, https://doi.org/10.1021/acs.analchem.0c02233.
[11] A. Nomura, K. Ito, D.Y.W. Yu, Y. Kubo, Gravimetric analysis of lithium-air batteries during discharge/charge cycles, J. Power Sources 592 (2024) 233924, https://doi.org/10.1016/j.jpowsour.2023.233924.
[12] E. Pastor, Z. Lian, L. Xia, D. Ecija, J.R. Galán-Mascarós, S. Barja, S. Giménez, J. Arbiol, N. López, García de Arquer, F. P. Complementary probes for the electrochemical interface, Nat. Rev. Chem. 8 (3) (2024) 159–178, https://doi.org/10.1038/s41570-024-00575-5.
[13] A. Cuesta, ATR-SEIRAS for time-resolved studies of electrode–electrolyte interfaces, Curr. Opin. Electrochem. 35 (2022) 101041, https://doi.org/10.1016/j.coelec.2022.101041.
[14] D. Neubauer, J. Scharpf, A. Pasquarelli, B. Mizaikoff, C. Kranz, Combined in situ atomic force microscopy and infrared attenuated total reflection spectroelectrochemistry, Analyst 138 (22) (2013) 6746–6752, https://doi.org/10.1039/c3an01169k.
[15] B.F. Baggio, Y. Grunder, In Situ X-ray techniques for electrochemical interfaces, Annu. Rev. Anal. Chem. 14 (1) (2021) 87–107, https://doi.org/10.1146/annurev-anchem-091020-100631.
[16] W.W. Wang, H. Yan, Y. Gu, J. Yan, B.W. Mao, In situ electrochemical atomic force microscopy: from interfaces to interphases, Annu. Rev. Anal. Chem. 17 (1) (2024) 103–126, https://doi.org/10.1146/annurev-anchem-061422-020428.
[17] X. Shi, W. Qing, T. Marhaba, W. Zhang, Atomic force microscopy - scanning electrochemical microscopy (AFM-SECM) for nanoscale topographical and electrochemical characterization: principles, applications and perspectives, Electrochim. Acta 332 (2020) 135472, https://doi.org/10.1016/j.electacta.2019.135472.
[18] M.D. Levi, L. Daikhin, D. Aurbach, V. Presser, Quartz Crystal Microbalance with Dissipation monitoring (EQCM-D) for in-situ studies of electrodes for supercapacitors and batteries: a mini-review, Electrochem. Commun. 67 (2016) 16–21, https://doi.org/10.1016/j.elecom.2016.03.006.
[19] G. Sauerbrey, Verwendung von Schwingquarzen zur Wägung dünner Schichten und zur Mikrowägung, Z. Phys. 155 (2) (1959) 206–222, https://doi.org/10.1007/bf01337937.
[20] D. Johannsmann, The Quartz Crystal Microbalance in Soft Matter Research, Springer International Publishing: Cham, 2015, https://doi.org/10.1007/978-3-319-07836-6.
[21] B. Rubin, J.L. Topper, C.C. Farnell, A.P. Yalin, Quartz crystal microbalance-based system for high-sensitivity differential sputter yield measurements, Rev. Sci. Instrum. 80 (10) (2009) 103506, https://doi.org/10.1063/1.3249560.
[22] P. Oberg, J. Lingensjo, Crystal film thickness monitor, Rev. Sci. Instrum. 30 (11) (1959) 1053, https://doi.org/10.1063/1.1716421.
[23] K.K. Kanazawa, J.G. Gordon, Frequency of a quartz microbalance in contact with liquid, Anal. Chem. 57 (8) (1985) 1770–1771, https://doi.org/10.1021/ac00285a062.
[24] I. Reviakine, D. Johannsmann, R.P. Richter, Hearing what you cannot see and visualizing what you hear: interpreting quartz crystal microbalance data from solvated interfaces, Anal. Chem. 83 (23) (2011) 8838–8848, https://doi.org/10.1021/ac201778h.
[25] N. Alanazi, M. Almutairi, A.N. Alodhayb, A review of quartz crystal microbalance for chemical and biological sensing applications, Sens. Imaging 24 (1) (2023) 10, https://doi.org/10.1007/s11220-023-00413-w.
[26] D.A. Buttry, M.D. Ward, Measurement of interfacial processes at electrode surfaces with the electrochemical quartz crystal microbalance, Chem. Rev. 92 (6) (1992) 1355–1379, https://doi.org/10.1021/cr00014a006.
[27] N. Shpigel, M.D. Levi, S. Sigalov, L. Daikhin, D. Aurbach, In Situ real-time mechanical and morphological characterization of electrodes for electrochemical energy storage and conversion by electrochemical quartz crystal microbalance with dissipation monitoring, Acc. Chem. Res. 51 (1) (2018) 69–79, https://doi.org/10.1021/acs.accounts.7b00477.
[28] Y. Ji, Z.-W. Yin, Z. Yang, Y.-P. Deng, H. Chen, C. Lin, L. Yang, K. Yang, M. Zhang, Q. Xiao, J.-T. Li, Z. Chen, S.-G. Sun, F. Pan, From bulk to interface: electrochemical phenomena and mechanism studies in batteries via electrochemical quartz crystal microbalance, Chem. Soc. Rev. 50 (19) (2021) 10743–10763, https://doi.org/10.1039/d1cs00629k.
[29] C. Leppin, A. Langhoff, O. Höfft, D. Johannsmann, A modulation QCM applied to copper electrodeposition and stripping, Electroanalysis no. 33 (12) (2021) 2529–2538, https://doi.org/10.1002/elan.202100471.
[30] C. Gabrielli, M. Keddam, R. Torresi, Calibration of the electrochemical quartz crystal microbalance, J. Electrochem. Soc. 138 (9) (1991) 2657–2660, https://doi.org/10.1149/1.2086033.
[31] J. Hu, S. Xue, O. Schneider, G. Yesilbas, A. Knoll, X. Huang, Comparison of the absolute mass sensitivity of ring electrode QCM and standard QCM using electrodeposition, Electroch. Commun. 119 (2020) 106826, https://doi.org/10.1016/j.elecom.2020.106826.
[32] J.-M. Friedt, K.H. Choi, F. Frederix, A. Campitelli, A.F.M. Simultaneous, Q.C. M. Measurements, J. Electrochem. Soc. 150 (10) (2003) H229, https://doi.org/10.1149/1.1603255.
[33] M. Edvardsson, S. Svedhem, G. Wang, R. Richter, M. Rodahl, B. Kasemo, QCM-D and reflectometry instrument: applications to supported lipid structures and their biomolecular interactions, Anal. Chem. 81 (1) (2009) 349–361, https://doi.org/10.1021/ac801523w.
[34] A.D. Easley, T. Ma, C.I. Eneh, J. Yun, R.M. Thakur, J.L. Lutkenhaus, A practical guide to quartz crystal microbalance with dissipation monitoring of thin polymer films, J. Polym. Sci. 60 (7) (2022) 1090–1107, https://doi.org/10.1002/pol.20210324.
[35] J.L.S. Antonio, V.L. Martins, S.I. Córdoba de Torresi, R.M. Torresi, QCM-D study of electrochemical synthesis of 3D polypyrrole thin films for negative electrodes in supercapacitors, Electrochim. Acta 324 (2019) 134887, https://doi.org/10.1016/j.electacta.2019.134887.
[36] M. Zhao, X. Tang, H. Zhang, C. Gu, Y. Ma, Characterization of complicated electropolymerization using UV–vis spectroelectrochemistry and an electrochemical quartz-crystal microbalance with dissipation: a case study of tricarbazole derivatives, Electrochem. Commun. 123 (2021) 106913, https://doi.org/10.1016/j.elecom.2020.106913.
[37] Y. Liu, B. Zhang, K.M. Gray, Y. Cheng, E. Kim, G.W. Rubloff, W.E. Bentley, Q. Wang, G.F. Payne, Electrodeposition of a weak polyelectrolyte hydrogel: remarkable effects of salt on kinetics, structure and properties, Soft Matter 9 (2013) 2703, https://doi.org/10.1039/c3sm27581g.
[38] K. Sadman, Q. Wang, S.H. Chen, D.E. Delgado, K.R. Shull, pH-controlled electrochemical deposition of polyelectrolyte complex films, Langmuir 33 (8) (2017) 1834–1844, https://doi.org/10.1021/acs.langmuir.6b04491.
[39] D. Martínez-Martín, G. Fläschner, B. Gaub, S. Martin, R. Newton, C. Beerli, J. Mercer, C. Gerber, D.J. Müller, Inertial picobalance reveals fast mass fluctuations in mammalian cells, Nature 550 (7677) (2017) 500–505, https://doi.org/10.1038/nature24288.
[40] I. Incaviglia, S. Herzog, G. Fläschner, N. Strohmeyer, E. Tosoratti, D.J. Müller, Tailoring the sensitivity of microcantilevers to monitor the mass of single adherent living cells, Nano Lett. 23 (2) (2023) 588–596, https://doi.org/10.1021/acs.nanolett.2c04198.
[41] D. Ramos, J. Tamayo, J. Mertens, M. Calleja, Photothermal excitation of microcantilevers in liquids, J. Appl. Phys. 99 (12) (2006), https://doi.org/10.1063/1.2205409.
[42] L.K. Ge, A. Tuniz, C.M. de Sterke, J.M. Zavislan, T.G. Brown, S. Martin, D. Martínez-Martín, Optimization and artifacts of photothermal excitation of microresonators, Adv. Sens. Res. 3 (8) (2024) 2300136, https://doi.org/10.1002/adsr.202300136.
[43] G. Meyer, N.M. Amer, Novel optical approach to atomic force microscopy, Appl. Phys. Lett. 53 (12) (1988) 1045–1047, https://doi.org/10.1063/1.100061.
[44] A.P. Cuny, K. Tanuj Sapra, D. Martínez-Martín, G. Fläschner, J.D. Adams, S. Martin, C. Gerber, F. Rudolf, D.J. Müller, High-resolution mass measurements of single budding yeast reveal linear growth segments, Nat. Commun. 13 (1) (2022) 3483, https://doi.org/10.1038/s41467-022-30781-y.
[45] S. Herzog, G. Fläschner, I. Incaviglia, J.C. Arias, A. Ponti, N. Strohmeyer, M. M. Nava, D.J. Müller, Monitoring the mass, eigenfrequency, and quality factor of mammalian cells, Nat. Commun. 15 (1) (2024) 1751, https://doi.org/10.1038/s41467-024-46056-7.
[46] F. Colombo, M. Villiou, F. Taheri, L. Fröhlich, M. Taale, V. Albert, Q. Jiang, C. Selhuber-Unkel, Fluctuations of dry and total mass of cells exposed to different molecular weights of polyethylene glycol, Adv. Nanobiomed. Res. 3 (7) (2023) 2200156, https://doi.org/10.1002/anbr.202200156.
[47] J. Zhu, Y. Tong, Z. Wang, Z. Li, L. Zhang, X. Guo, L. Tong, P. Wang, Gold flake-enabled miniature capacitive picobalances, Small Methods 9 (7) (2024), https://doi.org/10.1002/smtd.202401640 e2401640.
[48] W. Yu, J. Zhu, Y. Xu, X. Tu, Y. Tong, Y. Xie, P. Wang, L. Tong, L. Zhang, Optical nanofiber-enabled self-detection picobalance, ACS Photonics 11 (6) (2024) 2316–2323, https://doi.org/10.1021/acsphotonics.4c00216.
[49] A. Karg, T. Rößler, A. Mark, P. Markus, T. Lauster, N. Helfricht, G. Papastavrou, A versatile and simple approach to electrochemical colloidal probes for direct force measurements, Langmuir 37 (46) (2021) 13537–13547, https://doi.org/10.1021/acs.langmuir.1c01557.
[50] P. Knittel, H. Zhang, C. Kranz, G.G. Wallace, M.J. Higgins, Probing the PEDOT:PSS/cell interface with conductive colloidal probe AFM-SECM, Nanoscale 8 (2016) 4475–4481, https://doi.org/10.1039/c5nr07155k.
[51] Z. Schofield, G.N. Meloni, P. Tran, C. Zerfass, G. Sena, Y. Hayashi, M. Grant, S. A. Contera, S.D. Minteer, M. Kim, A. Prindle, P. Rocha, M.B.A. Djamgoz, T. Pilizota, P.R. Unwin, M. Asally, O.S. Soyer, Bioelectrical understanding and engineering of cell biology, J. R. Soc. Interface 17 (166) (2020) 20200013, https://doi.org/10.1098/rsif.2020.0013.
[52] G. Zhang, M. Levin, Bioelectricity is a universal multifaced signaling cue in living organisms, Mol. Biol. Cell 36 (2) (2025), https://doi.org/10.1091/mbc.E23-08-0312.
[53] D. Johannsmann, I. Reviakine, Quartz crystal microbalance with dissipation monitoring for studying soft matter at interfaces, Nature Rev. Meth. Primers 4 (1) (2024), https://doi.org/10.1038/s43586-024-00340-4.
[54] J.P. Cleveland, S. Manne, D. Bocek, P.K. Hansma, A nondestructive method for determining the spring constant of cantilevers for scanning force microscopy, Rev. Sci. Instrum. 64 (2) (1993) 403–405, https://doi.org/10.1063/1.1144209.
[55] J.R. Rumble, CRC Handbook of Chemistry and Physics, 105th Edition, CRC Press, Boca Raton, 2024.
[56] J.D. Adams, P.L.T.M. Frederix, C.A. Bippes, Breakthrough instruments and products: DriveAFM for high-performance atomic force microscopy, Rev. Sci. Instrum. 92 (12) (2021) 129503, https://doi.org/10.1063/5.0081190.
[57] J. Schindelin, I. Arganda-Carreras, E. Frise, V. Kaynig, M. Longair, T. Pietzsch, S. Preibisch, C. Rueden, S. Saalfeld, B. Schmid, J.Y. Tinevez, D.J. White, V. Hartenstein, K. Eliceiri, P. Tomancak, A. Cardona, Fiji: an open-source platform

for biological-image analysis, Nat. Methods 9 (7) (2012) 676–682, https://doi.org/10.1038/nmeth.2019.
[58] A.P. Cuny, D. Martínez-Martín, G. Fläschner, Automated analysis of inertial mass measurements of single cells, Software X 10 (2019) 100303, https://doi.org/10.1016/j.softx.2019.100303.
[59] G. Caniglia, S. Horn, C. Kranz, Scanning electrochemical probe microscopy: towards the characterization of micro- and nanostructured photocatalytic materials, Faraday Discuss. 257 (2025) 224–239, https://doi.org/10.1039/d4fd00136b.
[60] C. Kranz, G. Friedbacher, B. Mizaikoff, A. Lugstein, J. Smoliner, E. Bertagnolli, Integrating an ultramicroelectrode in an AFM cantilever: combined technology for enhanced information, Anal. Chem. 73 (11) (2001) 2491–2500, https://doi.org/10.1021/ac001099v.
[61] A. Karg, V. Kuznetsov, N. Helfricht, M. Lippitz, G. Papastavrou, Electrochemical grippers based on the tuning of surface forces for applications in micro- and nanorobotics, Sci. Rep. 13 (1) (2023) 7885, https://doi.org/10.1038/s41598-023-33654-6.
[62] S. Daboss, P. Knittel, C.E. Nebel, C. Kranz, Multifunctional boron-doped diamond colloidal AFM probes, Small 15 (48) (2019) e1902099, https://doi.org/10.1002/smll.201902099.
[63] S. Daboss, J. Lin, M. Godejohann, C. Kranz, Redox switchable polydopamine-modified AFM-SECM probes: a probe for electrochemical force spectroscopy, Anal. Chem. 92 (12) (2020) 8404–8413, https://doi.org/10.1021/acs.analchem.0c00995.
[64] A.E. Lindsay, D. O'Hare, A comparative study of thin film insulation techniques for gold electrodes, Electrochim. Acta 51 (28) (2006) 6572–6579, https://doi.org/10.1016/j.electacta.2006.04.052.
[65] J. Sripirom, S. Kuhn, U. Jung, O. Magnussen, A. Schulte, Pointed carbon fiber ultramicroelectrodes: a new probe option for electrochemical scanning tunneling microscopy, Anal. Chem. 85 (2) (2013) 837–842, https://doi.org/10.1021/ac3028432.
[66] S.N. Thorgaard, P. Bühlmann, Cathodic electropaint insulated tips for electrochemical scanning tunneling microscopy, Anal. Chem. 79 (23) (2007) 9224–9228, https://doi.org/10.1021/ac071307k.
[67] E.A. Hussein, B. Rice, R.J. White, Tuning the probe-bilayer architecture of silver nanoneedle-based ion channel probes, Langmuir (2024), https://doi.org/10.1021/acs.langmuir.4c00454.
[68] P.S. Dobson, J.M. Weaver, M.N. Holder, P.R. Unwin, J.V. Macpherson, Characterization of batch-microfabricated scanning electrochemical-atomic force microscopy probes, Anal. Chem. 77 (2) (2005) 424–434, https://doi.org/10.1021/ac048930e.
[69] M.R. Nellist, Y. Chen, A. Mark, S. Gödrich, C. Stelling, J. Jiang, R. Poddar, C. Li, R. Kumar, G. Papastavrou, M. Retsch, B.S. Brunschwig, Z. Huang, C. Xiang, S. W. Boettcher, Atomic force microscopy with nanoelectrode tips for high resolution electrochemical, nanoadhesion and nanoelectrical imaging, Nanotechnology 28 (9) (2017) 095711, https://doi.org/10.1088/1361-6528/aa5839.
[70] H. Shin, P.J. Hesketh, B. Mizaikoff, C. Kranz, Batch fabrication of atomic force microscopy probes with recessed integrated ring microelectrodes at a wafer level, Anal. Chem. 79 (13) (2007) 4769–4777, https://doi.org/10.1021/ac070598u.
[71] M.V. Mirkin, S. Amemiya (Eds.), Nanoelectrochemistry, CRC Press, 2015, https://doi.org/10.1201/b18066.
[72] B.A. Bircher, L. Duempelmann, K. Renggli, H.P. Lang, C. Gerber, N. Bruns, T. Braun, Real-time viscosity and mass density sensors requiring microliter sample volume based on nanomechanical resonators, Anal. Chem. 85 (18) (2013) 8676–8683, https://doi.org/10.1021/ac4014918.
[73] T. Braun, V. Barwich, M.K. Ghatkesar, A.H. Bredekamp, C. Gerber, M. Hegner, H. P. Lang, Micromechanical mass sensors for biomolecular detection in a physiological environment, Phys. Rev. Stat. Nonlin. Soft. Matter. Phys. 72 (3 Pt 1) (2005) 031907, https://doi.org/10.1103/PhysRevE.72.031907.
[74] C.P. Green, H. Lioe, J.P. Cleveland, R. Proksch, P. Mulvaney, J.E. Sader, Normal and torsional spring constants of atomic force microscope cantilevers, Rev. Sci. Instrum. 75 (6) (2004) 1988–1996, https://doi.org/10.1063/1.1753100.
[75] J.L. Hazel, V.V. Tsukruk, Spring constants of composite ceramic/gold cantilevers for scanning probe microscopy, Thin Solid Films 339 (1–2) (1999) 249–257, https://doi.org/10.1016/s0040-6090(98)00961-4.
[76] J.E. Sader, I. Larson, P. Mulvaney, L.R. White, Method for the calibration of atomic force microscope cantilevers, Rev. Sci. Instrum. 66 (7) (1995) 3789–3798, https://doi.org/10.1063/1.1145439.
[77] G. Fläschner, C.I. Roman, N. Strohmeyer, D. Martínez-Martín, D.J. Müller, Rheology of rounded mammalian cells over continuous high-frequencies, Nat. Commun. 12 (1) (2021) 2922, https://doi.org/10.1038/s41467-021-23158-0.
[78] Y.D. Gamburg, G. Zangari, Theory and Practice of Metal Electrodeposition, Springer, New York, 2011, https://doi.org/10.1007/978-1-4419-9669-5.
[79] D. Kramer, R.N. Viswanath, J. Weissmüller, Surface-stress induced macroscopic bending of nanoporous gold cantilevers, Nano Lett. 4 (5) (2004) 793–796, https://doi.org/10.1021/nl049927d.
[80] F. Tian, J.H. Pei, D.L. Hedden, G.M. Brown, T. Thundat, Observation of the surface stress induced in microcantilevers by electrochemical redox processes, Ultramicroscopy 100 (3–4) (2004) 217–223, https://doi.org/10.1016/j.ultramic.2003.12.012.
[81] R. Raiteri, H.-J. Butt, Measuring electrochemically induced surface stress with an atomic force microscope, J. Phys. Chem. 99 (43) (1995) 15728–15732, https://doi.org/10.1021/j100043a008.
[82] E. Gileadi, V. Tsionsky, Studies of electroplating using an EQCM. I. Copper and silver on gold, J. Electroch. Soc. 147 (2) (2000) 567, https://doi.org/10.1149/1.1393234.
[83] L. Daikhin, E. Gileadi, G. Katz, V. Tsionsky, M. Urbakh, D. Zagidulin, Influence of roughness on the admittance of the quartz crystal microbalance immersed in liquids, Anal. Chem. 74 (3) (2002) 554–561, https://doi.org/10.1021/ac0107610.
[84] J. te Riet, A.J. Katan, C. Rankl, S.W. Stahl, A.M. van Buul, I.Y. Phang, A. Gomez-Casado, P. Schön, J.W. Gerritsen, A. Cambi, A.E. Rowan, G.J. Vancso, P. Jonkheijm, J. Huskens, T.H. Oosterkamp, H. Gaub, P. Hinterdorfer, C.G. Figdor, S. Speller, Interlaboratory round robin on cantilever calibration for AFM force spectroscopy, Ultramicroscopy 111 (12) (2011) 1659–1669, https://doi.org/10.1016/j.ultramic.2011.09.012.
[85] M.K. Ghatkesar, V. Barwich, T. Braun, J.-P. Ramseyer, C. Gerber, M. Hegner, H. P. Lang, U. Drechsler, M. Despont, Higher modes of vibration increase mass sensitivity in nanomechanical microcantilevers, Nanotechnology 18 (44) (2007) 445502, https://doi.org/10.1088/0957-4484/18/44/445502.
[86] J.L. Hutter, J. Bechhoefer, Calibration of atomic-force microscope tips, Rev. Sci. Instrum. 64 (7) (1993) 1868–1873, https://doi.org/10.1063/1.1143970.
[87] M. Edvardsson, Application note: the Sauerbrey equation, Biolin Sci. (2025). https://content.biolinscientific.com/overview-the-sauerbrey-relation.
[88] C.D. McCaig, B. Song, A.M. Rajnicek, Electrical dimensions in cell science, J. Cell Sci. 122 (23) (2009) 4267–4276, https://doi.org/10.1242/jcs.023564.
[89] C. Chen, X. Bai, Y. Ding, I.S. Lee, Electrical stimulation as a novel tool for regulating cell behavior in tissue engineering, Biomater. Res. 23 (1) (2019) 25, https://doi.org/10.1186/s40824-019-0176-8.
[90] Y. Wang, M. Rouabhia, D. Lavertu, Z. Zhang, Pulsed electrical stimulation modulates fibroblasts' behaviour through the Smad signalling pathway, J. Tissue Eng. Regen. Med. 11 (4) (2017) 1110–1121, https://doi.org/10.1002/term.2014.
[91] R.S. Barman, S. Jhunjhunwala, Electrical stimulation for immunomodulation, ACS Omega 9 (1) (2024) 52–66, https://doi.org/10.1021/acsomega.3c06696.
[92] D. Czerwińska-Glówka, K. Krukiewicz, A journey in the complex interactions between electrochemistry and bacteriology: from electroactivity to electromodulation of bacterial biofilms, Bioelectrochemistry 131 (2020) 107401, https://doi.org/10.1016/j.bioelechem.2019.107401.